Journal of Applied Electrochemistry **30**: 173–179, 2000.

Normal and anomalous codeposition of Zn–Ni alloys from chloride bath

G. ROVENTI[1], R. FRATESI[1*], R.A. DELLA GUARDIA[1] and G. BARUCCA[2]
[1]*Dipartimento di Scienze dei Materiali e della Terra, Università degli Studi di Ancona. Via Brecce Bianche, 60131 Ancona, Italy*
[2]*INFM, Università degli Studi di Ancona. Via Brecce Bianche, 60131 Ancona, Italy*
*(*author for correspondence)*

Received 15 April 1999; accepted in revised form 20 July 1999

Key words: alloys, electrodeposition, nickel, zinc

Abstract

The codeposition of Zn–Ni alloys from chloride bath has been studied by means of potentiostatic electrodeposition in the potential range −700 to −1100 mV vs Ag/AgCl, where both normal and anomalous codeposition occurs. Deposition of alloys of different composition, morphology and structure, depending on the cathodic potential, was found. Analysis of the partial current densities showed that the production of nickel rich alloys in the potential range −700 to −900 mV is due to the underpotential reduction of zinc, driven by nickel ion discharge. Morphological and microstructural analyses showed that these alloys have the face-centred-cubic structure of nickel (α phase) and that the addition of zinc in the nickel lattice causes internal stresses in the deposits, which are prevalently amorphous. At potentials more negative than −910 mV, corresponding to the equilibrium potential of the zinc rich γ phase deposition, the rate of deposition of the α phase decreases and the further increase in deposit zinc content leads to the formation of the γ phase, with a decrease in internal stress. In this range of potential, zinc and nickel reduction can occur separately, according to their respective exchange current densities.

1. Introduction

The electrodeposition of zinc alloys with group eight metals (Ni, Co and Fe) has recently attracted interest because of their high corrosion resistance compared to that of pure zinc [1]. In particular, Zn–Ni alloy coatings are considered a less polluting alternative to cadmium, already in decline due to its toxicity [2].

The electrodeposition of Zn–Ni alloys is generally a codeposition of anomalous type, according to Brenner's definition [3], since the less noble metal zinc deposits preferentially and its percentage in the deposit is higher than that in the electrolyte. However, normal Zn–Ni codepositon is possible in particular experimental conditions [4–6]. Many attempts have been made to explain the anomalous codeposition of alloys, but there is still no universally accepted theory. At first, anomalous codeposition was attributed to the pH increase at the cathode surface being able to induce zinc hydroxide precipitation, which inhibits nickel discharge [4, 5, 7, 8]. This theory does not explain the strong inhibition of nickel reduction observed in the normal deposition region, the high current efficiency during anomalous codeposition and the increase in nickel content in the alloy with increasing pH [9]. Another theory [10, 11] assumes that anomalous codeposition is due to the underpotential deposition (upd) of zinc, but usually anomalous deposition occurs in the zinc overpotential deposition region. Recently, Zn–Ni codeposition was studied by means of polarization curves and impedance spectroscopy measurements both in chloride [12] and in sulphate bath [9, 13]. Even though metal cations can form chloro-complexes in chloride electrolyte [14], in contrast to what happens in sulphate electrolyte, the reaction models proposed are substantially similar and involve several adsorbed intermediates. In particular, at low cathodic polarization (normal codeposition) the deposition of nickel-rich alloys was attributed to a mixed intermediate ($ZnNi^{+}_{ad}$), which catalyses the reduction of Ni^{2+} ions. At high cathodic polarizations (anomalous codeposition) zinc preferential discharge is attributed to the intermediate Zn^{+}_{ads}, catalyst for the deposition of zinc rich deposits.

Previously [6, 15, 16], anomalous codepositions of Zn–Ni alloy from chloride bath containing NH_4Cl and Zn–Co alloy from simple chloride bath have been treated, emphasizing the difference between the very low exchange current densities of the iron group metals with respect to that of zinc. For Zn–Co potentiostatic deposition over a wide range of potential [15], it was found that the trend in the cobalt partial current density is related to changes in composition, structure and morphology of the alloys obtained at the different potentials. It was also found that, at low polarization,

the upd discharge of zinc is driven by cobalt ion reduction. The aim of the present work on Zn–Ni alloy codeposition was to confirm the results obtained previously for Zn–Co alloys. Therefore, Zn–Ni alloy potentiostatic electrodeposition was carried out from chloride bath without NH_4Cl in the potential range -700 to -1100 mV vs Ag/AgCl, where both normal and anomalous codeposition occurs.

2. Experimental details

Zn–Ni alloys were obtained at various temperatures (25, 40 and 55 °C), under potentiostatic conditions using baths of the following composition: $ZnCl_2$ 7.8–64.4 g dm^{-3} (0.06–0.47 M); $NiCl_2.6H_2O$ 136.2–26.5 g dm^{-3} (0.57–0.11 M); H_3BO_3 26 g dm^{-3}; KCl 220 g dm^{-3}; pH 4.8. Zinc and nickel percentages in the bath were changed, while the total metal concentration was kept constant (M_{tot} 37.4 g dm^{-3}). Pure nickel or zinc deposition was also carried out from baths containing 37.4 g dm^{-3} in Ni or Zn. Some pure metal depositions were carried out with the same bath concentrations used for the alloy depositions. To maintain the total metal concentration constant, one of the metals was substituted with an equal concentration of $MgCl_2.6H_2O$ [17]. All the solutions were prepared with doubly distilled water and analytical grade reagents.

Electrodeposits were obtained on mild steel discs, 1 mm thick (exposed area 3.46 cm^2). Before electrodeposition, the samples were polished with emery paper and any grease was removed from the surfaces by anodic and cathodic electrolysis for 2 min in an aqueous 60 g dm^{-3} NaOH solution at 4 V against graphite anodes. The samples were then neutralised in a 2% HCl solution and rinsed with distilled water. A glass cell 1 dm^{-3} in capacity was used. The anode was a zinc sheet (total area 50 cm^2). Before immersion in the bath, the zinc anode was immersed in a solution of similar composition at 40 °C for 3 h, without current flow. The zinc sheet was coated with a dark nickel layer, which reduced both the depletion of nickel in the bath, due to its cementation on the zinc anode, and the enrichment in zinc in the bath, due to the strong dissolution of the zinc anode. The deposition potential was controlled by a High Power Potentiostat AMEL model 2055 with Ag/AgCl as reference electrode, mounted in a Luggin capillary, and the amount of electrical charge was recorded to calculate the average current density. During the electrodeposition the cathodic solution was mechanically stirred. After deposition, the disc cathodes were thoroughly washed with water and then ethanol, hot air dried and weighed.

To determine the percentage composition of the electrodeposited alloys, the deposits were stripped in a minimum volume of 1:3 HCl solution and analysed for nickel and zinc using an inductively coupled plasma spectrometer (Perkin-Elmer Optima 3200 XL). By means of Faraday's law, the partial current densities of zinc, nickel and hydrogen were calculated. In order to study the deposit morphology, scanning electron microscopy (SEM) was performed on a Philips XL 20 instrument. The deposited phases were analysed by means of a Philips PW1730 X-ray diffractometer, using CuK_α ($\lambda = 154.056$ pm) radiation and by a Philips CM 200 transmission electron microscope (TEM), equipped with a LaB_6 filament.

3. Results and discussion

Figure 1 shows the polarization curves for potentiostatic electrodeposition carried out at 55 °C, using baths containing different nickel percentages and baths with only nickel or zinc ions. Zinc deposition from baths containing only zinc ions starts at about -1000 mV; at higher potentials cathode surface analysis did not reveal the presence of zinc, indicating that the current is due to hydrogen discharge. Alloy deposition is strongly inhibited compared to that of pure nickel, but is enhanced compared to pure zinc deposition at potentials above -1000 mV. The nickel and zinc partial current density curves obtained from the bath containing 30% Ni and the curves of pure Ni and Zn deposition from baths having the same concentrations (Figure 2) show that zinc can be codeposited with nickel at potentials where it does not deposit in pure form. These results agree with the formation, at low cathodic polarization, of a mixed intermediate which catalyses the deposition of nickel rich phases, as proposed by Fabri Miranda et al. [14]. Similarly to induced codeposition, where a given element can be codeposited to form an alloy, but cannot be deposited in pure form, interactions between the components in the deposit may shift the deposition potential of the less noble metal [18].

The percentages of nickel in the alloys deposited at various potentials are shown in Figure 3. The deposits obtained from the bath containing 90% Ni were cracked

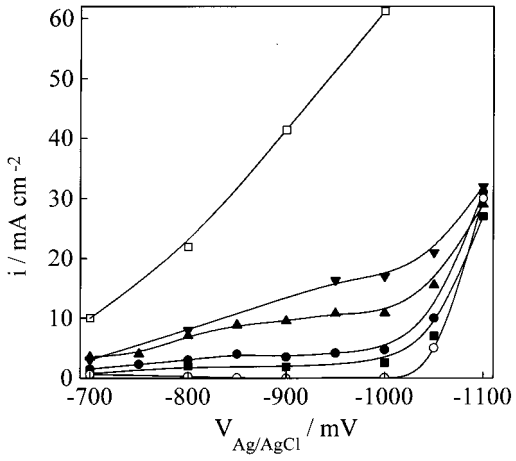

Fig. 1. Polarization curves for potentiostatic depositions carried out from baths containing the following percentages of nickel (Ni_b): (□) 100%; (▼) 85%; (▲) 60%; (●) 30%; (■) 17.5%; (○) 0%. $T = 55$ °C.

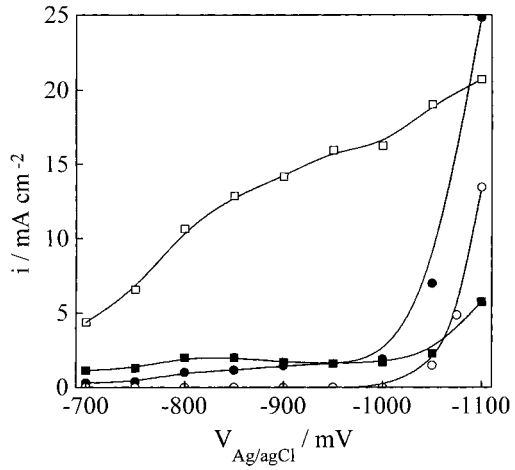

Fig. 2. Partial current densities for nickel and zinc as a function of applied potential during Zn–Ni alloy deposition (bath containing 30% Ni) and pure metal deposition from baths containing the same zinc or nickel concentrations. Ni^{2+} 0.19 M; Zn^{2+} 0.40 M; $T = 55\,^{\circ}C$. (□) i_{Ni}, pure nickel deposition; (■) i_{Ni}, alloy deposition; (○) i_{Zn}, pure zinc deposition; (●) i_{Zn}, alloy deposition.

even when very thin and it was not possible to obtain reproducible results at potentials lower than −950 mV. On increasing the nickel bath concentration, the change in composition of the deposits became gradually less dependent on the applied potential. The letters (a), (b) and (c) indicate alloys with the same percentage of nickel in the bath, that is the points where the transition from normal to anomalous occurs. On increasing the nickel percentage in the bath, the transition occurs at more positive potentials; the codeposition is anomalous at all potentials for the baths containing 85 and 90% Ni are. These results indicate that high nickel bath concentrations promote anomalous codeposition.

Figure 4 shows the effect of temperature on the polarization curves and nickel percentages in the deposits. The increase in temperature from 25 to 55 °C does not significantly change the composition of the deposits, which depends mainly on the potential, but leads to an increase in the deposition current density. As previously found [6], the temperature increase favours nickel reduction compared to that of zinc; at low polarization the increase in the whole process rate is due also to the increase in zinc discharge, driven by the discharge of nickel.

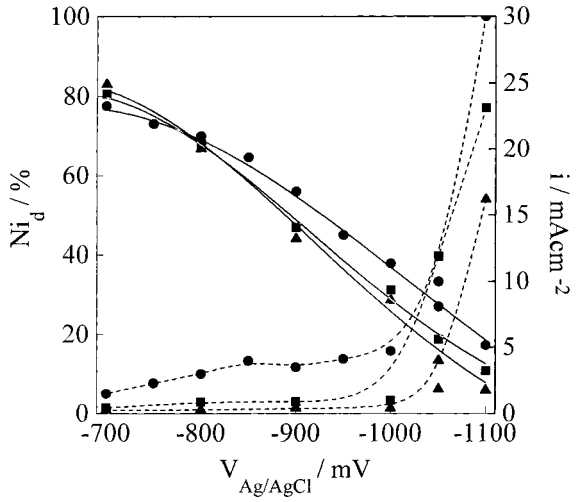

Fig. 4. Polarization curves (- - - -) and nickel percentages (——) in the deposits obtained at various temperatures, T: (●) 55, (■) 40 and (▲) 25 °C. Ni_b 30%.

Figure 5 shows the relation between alloy composition and solution composition at different potentials. The composition reference line (CRL) is also given. At a potential of −700 mV the alloy composition is almost constant and does not seem to depend on the bath composition; with decrease in the deposition potential the slope of the curves increases.

The partial current densities of zinc (i_{Zn}), nickel (i_{Ni}) and hydrogen (i_{H_2}) together with the total (i_{tot}) electrolysis current for the baths containing Ni 17.5%, 30% and

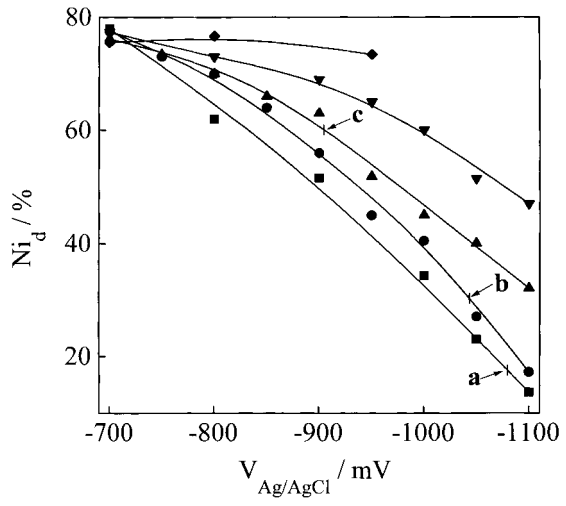

Fig. 3. Effect of potential on the percentage of nickel (Ni_d) in zinc–nickel alloys electrodeposited from baths containing the following percentages of nickel (Ni_b): (◆) 90%; (▼) 85%; (▲) 60%; (●) 30%; (■) 17.5%. $T = 55\,^{\circ}C$.

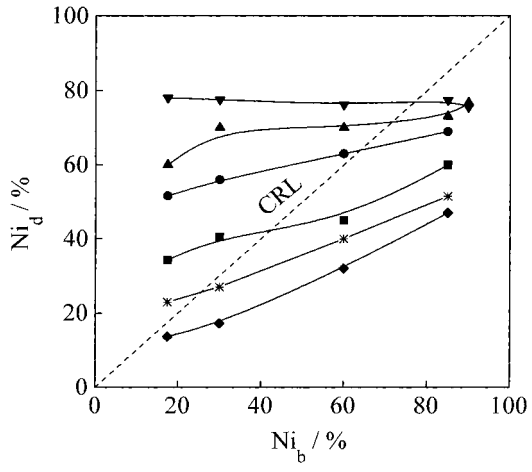

Fig. 5. Effect of the nickel percentage in the bath (Ni_b) on the nickel percentage of the deposits (Ni_d) obtained at the following potential values: (▼) −700, (▲) −800, (●) −900, (■) −1000, (∗) −1050 and (◆) −1100 mV. $T = 55\,^{\circ}C$.

60% are shown in Figure 6. The dotted lines indicate the potentials where the transition from normal to anomalous codeposition, as defined by Brenner [3], occurs; the transition does not seem to correlate with particular changes in the partial current densities and, therefore, with changes in the reaction mechanism. In fact, the trends of the partial current densities are substantially the same for the three baths studied and depend mainly on the potential, even though the transition occurs at different potentials. Similar results were also found by Elkhatabi et al. in Zn–Ni alloy deposition from NH_4Cl based baths [21]. On increasing the nickel concentration in the bath, i_{tot} increases markedly at potentials higher than -1000 mV, due principally to the increase in nickel partial current density which, in turn, causes an increase in the zinc partial current density. The hydrogen current density is low at all the potentials studied and no remarkable increase was found corresponding to the transition, in agreement with previous results [6, 15]. The nickel partial current density shows a maximum around -850 mV, followed by a minimum around -1000 mV. This trend is similar to that of the cobalt partial current density, obtained in Zn–Co alloy electrodeposition under the same experimental conditions [15], even though i_{Ni} are lower than i_{Co}, in agreement with their respective exchange current densities [19]. The zinc partial current density does not show a minimum, due to the onset of zinc rich γ phase deposition, which has an equilibrium potential of about -910 mV vs Ag/AgCl [20].

Figure 7 shows the ratio i_{Zn}/i_{Ni} as a function of the deposition potential. On changing the potential from -700 to -900 mV this ratio increases only slightly and does not seem to depend on bath composition. At potentials lower than about -900 mV the ratio increases and depends on the bath zinc content. It is noteworthy that up to -900 mV the ratio i_{Zn}/i_{Ni} is almost the same for all baths, even though the codeposition is anomalous for the bath containing 85% Ni and normal for the others. The present results lead to some doubts on Brenner's classification of Zn–Ni codeposition as normal at low polarization. Normal codeposition indicates, collectively, regular (under diffusion control), irregular (controlled by the idiosyncrasies of the potentials of the metals against the solution) and equilibrium (the ratios of the metals in the deposit is the same as their ratio in the bath) codeposition [3]. The present results, and those found previously for Zn–Co alloy deposition [15], do not agree with any of the mechanisms described above, but show that the production of Zn–Ni and Zn–Co alloys at low polarization is due to the underpotential discharge of Zn, driven by nickel or cobalt ion reduction. Only when the equilibrium potential of zinc rich phases is reached can zinc and nickel reduction occur separately, according to their respective exchange current densities.

Figure 8 shows the X-ray diffraction patterns of alloys obtained from the bath containing 30% Ni (curves (b)–(f)) at different potentials compared to the deposit obtained at -700 mV from the bath containing only nickel ions (curve (a)). All the deposits were about 3 μm thick. The pure nickel deposit is crystalline and Figure 9 shows its surface morphology. The addition of 22.5% Zn (Figure 10, alloy obtained at -700 mV) causes a

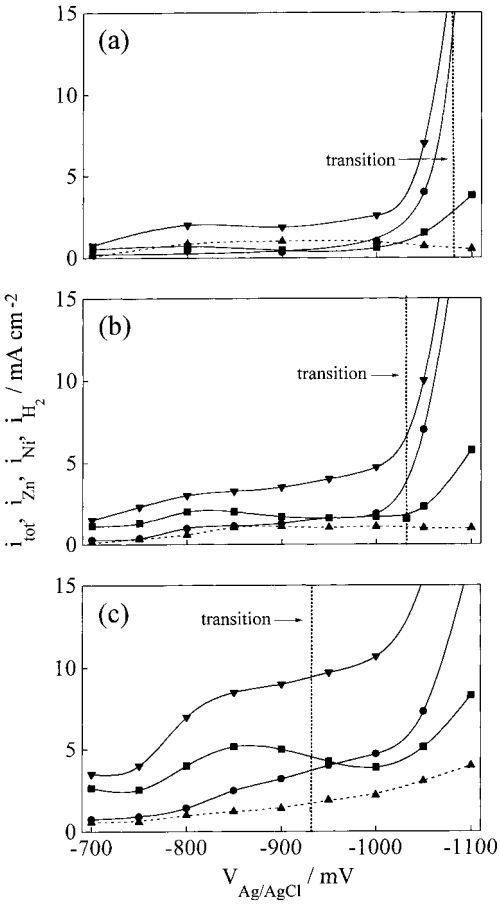

Fig. 6. Effect of the electrode potential on the partial current densities for nickel (■), zinc (●) and H_2 (▲) reduction, together with the total current density (▼). (a) bath with 17.5% Ni; (b) bath with 30% Ni; (c) bath with 60% Ni. $T = 55\,^{\circ}C$.

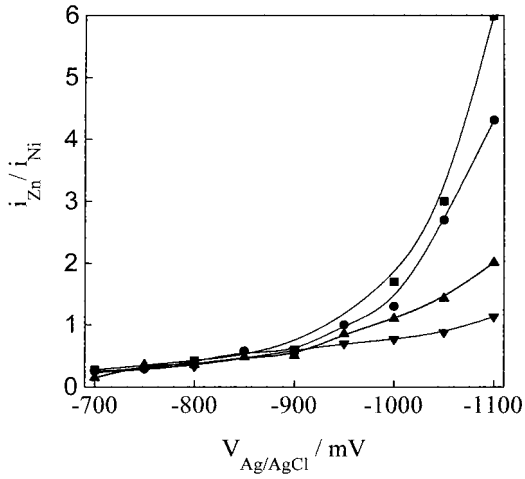

Fig. 7. Effect of the cathodic potential on the ratio i_{Zn}/i_{Ni} for baths containing the following nickel percentages: (▼) 85%, (▲) 60%, (●) 30% and (■) 17.5%. $T = 55\,^{\circ}C$.

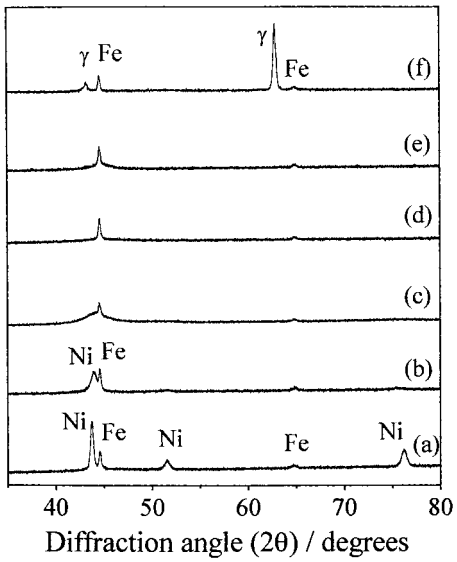

Fig. 8. X-ray diffraction patterns of Zn–Ni alloys obtained by potentiostatic electrodepositions: (a) −700 mV, bath without zinc; (b) −700 mV, Ni_b 30%; (c) −800 mV, Ni_b 30%; (d) −850 mV, Ni_b 30%; (e) −1000 mV, Ni_b 30%; (f) −1050 mV. Ni_b 30%. $T = 55\,^{\circ}C$.

surface smoothness, with the formation of few thin cracks. The corresponding diffraction pattern (Figure 8, curve (b)) gives, together with the peaks related to the substrate, only one peak corresponding to the main peak of pure nickel. This indicates that the addition of zinc does not change the face centred cubic (f.c.c.) structure of nickel, even though in the case of the alloy the peak is low and broad, suggesting that the deposit tends to become microcrystallized or amorphous. The increase in zinc content to 30.1% (Figure 11, deposit obtained at −800 mV) produces a smooth deposit showing some nodules on its surface, with an increase in the number and depth of cracks. The corresponding diffraction pattern (Figure 8, curve (c)) shows that the nickel peak becomes lower and broader, indicating that the structure is almost microcrystalline or amorphous.

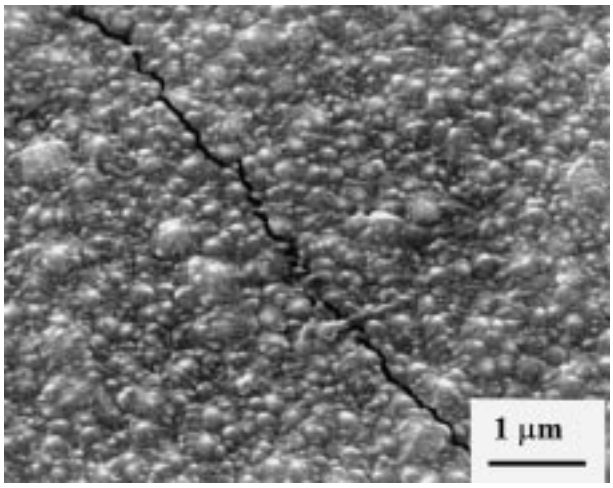

Fig. 10. Microstructure of the alloy obtained by potentiostatic electrodeposition at −700 mV. Ni_b 30%; $T = 55\,^{\circ}C$. Zn_d 22.5%.

TEM observations (Figure 12 (a)) show that the deposit is composed of crystals, whose dimensions range from 5 to about 100 nm, uniformly distributed in an amorphous matrix. To confirm the presence of an amorphous phase, the sample was tilted and electron microdiffraction analyses were performed. The electron diffraction pattern of the crystalline phase, obtained using a small selected area diaphragm to reduce the amorphous phase contribution, shows rings corresponding to the f.c.c. nickel interplanar distances (Figure 12 (b)). SEM observation on the deposit obtained at −850 mV, containing 35% Zn, shows that the nodules appear over the whole surface, together with many deep cracks, which indicate a high degree of brittleness (Figure 13). It is unlikely that the cracks are a result of hydrogen evolution, because there is no significant increase in the corresponding partial current density at this potential (Figure 6 (b)). The increase in zinc content to 35%, corresponding to the equilibrium solubility of zinc in the Ni α phase [12], is the more probable cause. The alloy

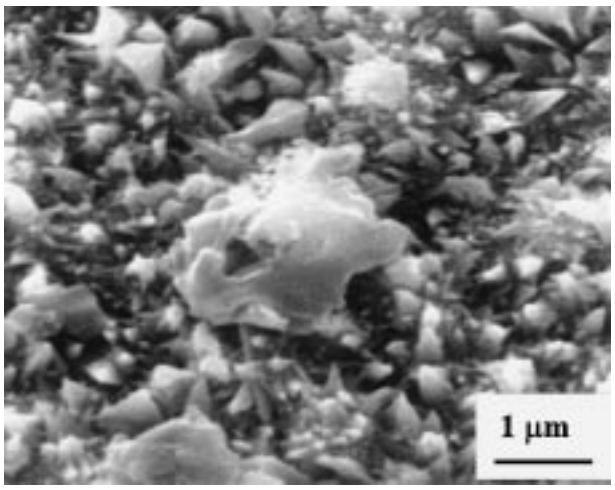

Fig. 9. Microstructure of the pure nickel deposit obtained by potentiostatic electrodeposition at −700 mV. Ni_b 37.4 g dm^{-3}. $T = 55\,^{\circ}C$.

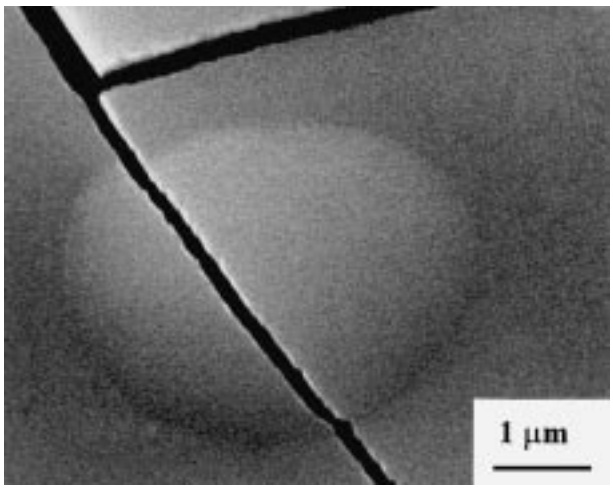

Fig. 11. Microstructure of the alloy obtained by potentiostatic electrodeposition at −800 mV. Ni_b 30%; $T = 55\,^{\circ}C$. Zn_d 30.1%.

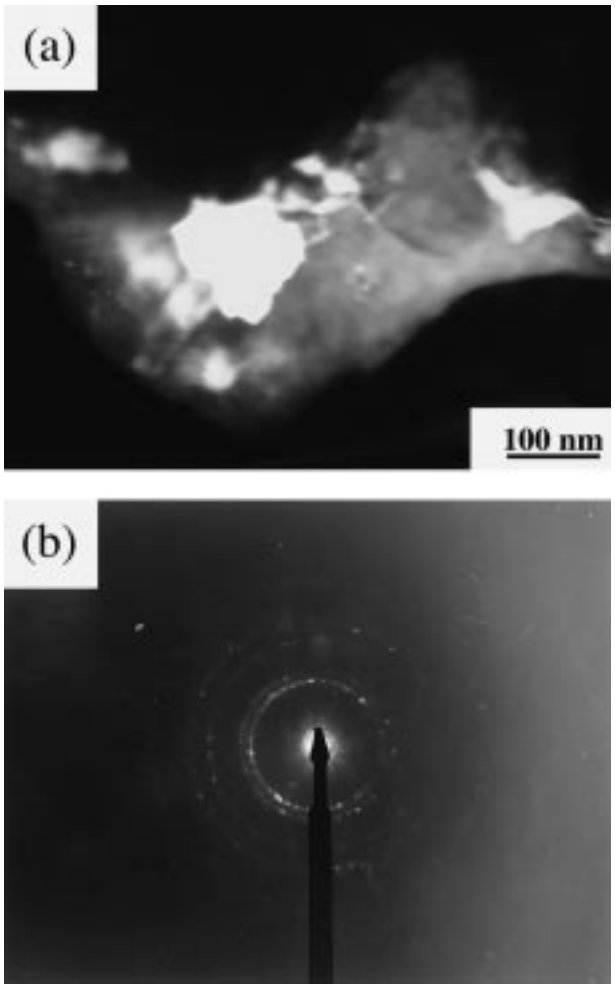

Fig. 12. (a): TEM image of the alloy of Figure 11 (dark field); (b): corresponding electron diffraction pattern.

obtained at −1000 mV (Figure 14) has about 60% Zn and its surface has fewer cracks and nodules; there is also an increase in surface roughness with respect to the deposit obtained at −850 mV. The X-ray spectra show that deposits obtained at −850 mV and at −1000 mV are

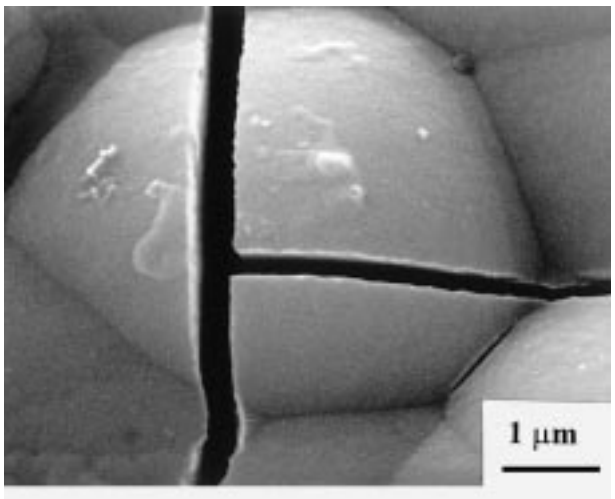

Fig. 13. Microstructure of the alloy obtained by potentiostatic electrodeposition at −850 mV. Ni_b 30%; $T = 55\,^{\circ}C$. Zn_d 35.0%.

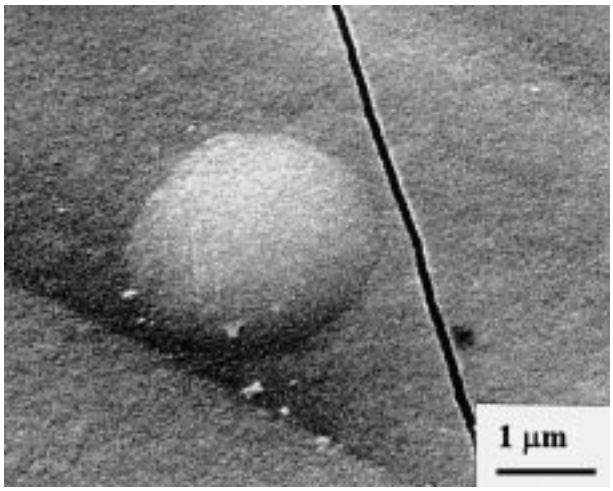

Fig. 14. Microstructure of the alloy obtained by potentiostatic electrodeposition at −1000 mV. Ni_b 30%; $T = 55\,^{\circ}C$. Zn_d 59.5%.

completely microcrystallized or amorphous (Figure 8, curves (d) and (e), respectively). TEM investigations performed on the last deposit reveal the presence of crystals uniformly distributed in an amorphous matrix (Figure 15 (a)); crystal dimensions range from 5 to 200 nm. Electron diffraction performed on the crystal-

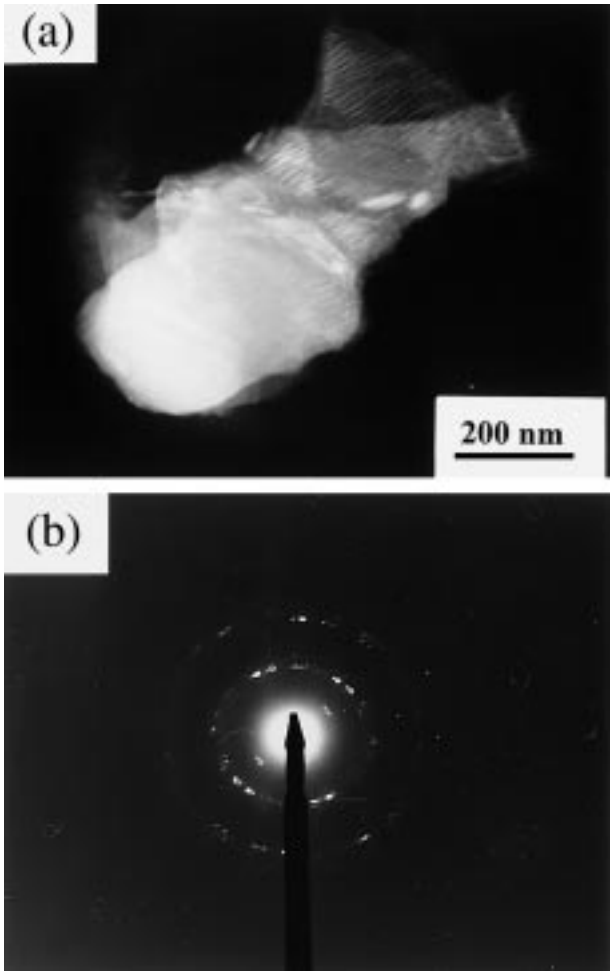

Fig. 15. (a): TEM image of alloy of Figure 15 (dark field); (b): corresponding electron diffraction pattern.

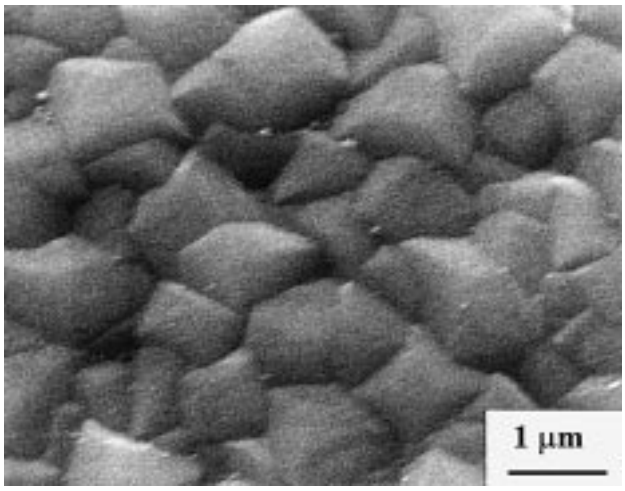

Fig. 16. Microstructure of the alloy obtained by potentiostatic electrodeposition at −1050 mV. Ni_b 30%; $T = 55\,^{\circ}C$. Zn_d 77.7%.

line phase (Figure 15 (b)) shows some rings which are not continuous, indicating an orientation relationship among the crystals. The interplanar distances connected to the most intense spots correspond to the γ phase (Ni_5Zn_{21}). At −1050 mV the zinc percentage reaches about 78% and the deposit consists of pyramidal crystallites (Figure 16). X-ray diffraction indicates that the deposit is crystalline and its structure is that of the γ phase (Figure 8, curve (f)).

These results show that the increase in zinc percentage in the alloys up to 35%, obtained by changing the potential from −700 to about −850 mV, leads to progressively more amorphous and stressed deposits. At more negative potentials, the percentage of zinc increases again, but the α phase deposition rate decreases, as indicated by the nickel partial current density decrease (Figure 6). When the potential of the γ phase deposition is reached, the further increase in zinc content leads to the formation of the zinc rich phase and to an increase in current density. The influence of potential on composition, structure and morphology of zinc–nickel alloys is very similar to that found previously for Zn–Co alloy deposition under the same experimental conditions [15]. A dependence of the morphology and structure of Zn–Ni alloys on the deposition potential was found also by other authors [21].

4. Conclusions

Zn–Ni alloy potentiostatic electrodepositions in the range −700 to −1100 mV Ag/AgCl showed that nickel deposition is strongly inhibited by the presence of zinc, while zinc deposition is enhanced by the presence of nickel at low polarization. The hydrogen partial current density was found to be low at all potentials and no remarkable increase was found in correspondence of the normal/anomalous codeposition transition, in agreement with previous results. Also, the transition does not seem to correlate with particular changes in the partial current densities, which depend mainly on the deposition potential.

Two different mechanisms depending on the potential can be hypothesized:

(i) At low polarization, the production of Zn–Ni alloys is due to the underpotential discharge of Zn, driven by nickel ion reduction. In the potential range −700 to about −900 mV the i_{Zn}/i_{Ni} ratio changes only slightly and does not depend on the bath composition. X-ray, SEM and TEM analyses show that the addition of zinc in the nickel lattice leads to progressively more amorphous and more stressed deposits. The maximum internal stress was found in deposits obtained at −850 mV and containing about 35% zinc, corresponding to the equilibrium solubility of zinc in the nickel rich α phase. At more negative potentials the increase in zinc content of the deposits leads to a decrease in the α phase deposition rate.

(ii) At potentials more negative than −910 mV, corresponding to the equilibrium potential of the zinc rich γ phase deposition, the further increase in zinc content of the deposits leads to the formation of the γ phase, with a decrease in internal stress. In this range of potential zinc and nickel reduction can occur separately, according to their respective exchange current densities.

References

1. D. Crotty, *Met. Finish.* **94** (1996) 54.
2. G.F. Hsu, *Plat. Surf. Finish.* **71** (1984) 52.
3. A. Brenner, '*Electrodeposition of Alloys*', Vol 1 and 2 (Academic Press, New York and London, 1963).
4. D.E. Hall, *Plat. Surf. Finish.* **71** (1983) 59.
5. H. Fukushima, T. Akiyama, K. Higashi, R. Kammel and M. Karimkhani, *Metall.* **42** (1988) 242.
6. R. Fratesi and G. Roventi, *J. Appl. Electrochem.* **22** (1992) 657.
7. H. Dahms and J.M. Croll, *J. Electrochem. Soc.* **112** (1965) 771.
8. S.S. Abd El Rehim, E.E. Fouad, S.M. Abd El Wahab and Hamdy. H. Hassan, *Electrochim. Acta* **41** (1996) 1413.
9. F.J. Fabri Miranda, O.E. Barcia, O.R. Mattos and R. Wiart, *J. Electrochem. Soc.* **144** (1997) 3441.
10. M.I. Nicol and H.I. Philip, *J. Electroanal. Chem.* **70** (1976) 233.
11. S. Swathirajan, *J. Electroanal. Chem.* **221** (1987) 211.
12. E. Chassaing and R. Wiart, *Electrochim. Acta* **37** (1992) 545.
13. F.J. Fabri Miranda, O.E. Barcia, O.R. Mattos and R. Wiart, *J. Electrochem. Soc.* **144** (1997) 3449.
14. M.F. Mathias and T.W. Chapman, *J. Electrochem. Soc.* **137** (1990) 102.
15. R. Fratesi, G. Roventi, G. Giuliani and C.R. Tomachuk, *J. Appl. Electrochem.* **27** (1997) 1088.
16. L. Felloni, R. Fratesi, E. Quadrini and G. Roventi, *J. Appl. Electrochem.* **17** (1987) 574.
17. D. Landolt, *Electrochim. Acta* **39** (1994) 1075.
18. E. Chassaing, K. Vu Quang and R. Wiart, *J. Appl. Electrochem.* **19** (1989) 893.
19. R. Fratesi and G. Roventi, *Mater. Chem. Phys.* **23** (1989) 529.
20. S. Swathirajan, *J. Electrochem. Soc.* **133** (1986) 671.
21. F. Elkhatabi, M. Benballa, M. Sarret, C. Müller, *Electrochim. Acta* **44** (1999) 1645.